A genetic mouse model of severe iron deficiency anemia reveals tissue-specific transcriptional stress responses and cardiac remodeling

Received for publication, May 29, 2019, and in revised form, August 13, 2019 Published, Papers in Press, August 15, 2019, DOI 10.1074/jbc.RA119.009578

Andrew J. Schwartz[‡], **Kimber Converso-Baran**[‡], **Daniel E. Michele**[‡§], **and Yatrik M. Shah**[‡¶1]

From the [‡]*Department of Molecular & Integrative Physiology, and Internal Medicine, Divisions of* [§]*Cardiovascular Medicine and* [¶]*Gastroenterology, University of Michigan, Ann Arbor, Michigan 48109*

Edited by Xiao-Fan Wang

Iron is a micronutrient fundamental for life. Iron homeostasis in mammals requires sustained postnatal intestinal iron absorption that maintains intracellular iron concentrations for central and systemic metabolism as well as for erythropoiesis and oxygen transport. More than 1 billion people worldwide suffer from iron deficiency anemia (IDA), a state of systemic iron insufficiency that limits the production of red blood cells and leads to tissue hypoxia and intracellular iron stress. Despite this tremendous public health concern, very few genetic models of IDA are available to study its progression. Here we developed and characterized a novel genetic mouse model of IDA. We found that tamoxifen-inducible deletion of the mammalian iron exporter ferroportin exclusively in intestinal epithelial cells leads to loss of intestinal iron absorption. Ferroportin ablation yielded a robust phenotype of progressive IDA that develops in as little as 3 months following disruption of intestinal iron absorption. We noted that, at end-stage IDA, tissue-specific transcriptional stress responses occur in which the heart shows little to no hypoxic and iron stress compared with other peripheral organs. However, morphometric and echocardiographic analysis revealed massive cardiac hypertrophy and chamber dilation, albeit with increased cardiac output at very low basal heart rates. We propose that our intestine-specific ferroportin knockout mouse model of end-stage IDA could be used in future studies to investigate IDA progression and cell-specific responses to hypoxic and iron stress.

Iron is an essential micronutrient to sustain life, from single-cell bacteria to complex multicellular organisms. In mammals, systemic iron homeostasis requires multiple organs working in concert to maintain red blood cell (RBC)[2] levels for oxygen transport and intracellular iron concentrations for redox and metabolic reactions (1). More than 2 billion people are affected by iron deficiency worldwide, and 1 billion suffer from iron deficiency anemia (IDA) (2). In IDA, iron absorption is limited to an extent that restricts the production of RBCs, ultimately leading to decreased transport of systemic oxygen and the development of intracellular iron stress (3). IDA is more common in developing countries, where it is mainly caused by inadequate dietary consumption of iron but also by blood loss because of intestinal worm colonization (4). In more developed countries, dietary eating habits, such as vegetarianism, as well as pathologic conditions that cause bleeding or malabsorption are common causes (4). Patients with IDA are typically treated with dietary iron. A significant number of IDA patients are refractory to oral iron supplementation, known as iron-refractory IDA (IRIDA) (5). IRIDA patients require intravenous iron supplementation. If uncorrected, IDA can result in severe fatigue, weakness, and pathological cardiac complications (6, 7).

Our group, among others, has unveiled that systemic iron homeostasis is regulated in mammals by a heterotissue crosstalk mechanism involving the liver-derived hormone hepcidin and the intestinal transcription factor hypoxia-inducible factor 2α (HIF-2α) (8–12). The function of hepcidin is to bind to the only mammalian iron exporter, ferroportin (Fpn), resulting in internalization from the plasma membrane, intracellular degradation, and an increase in intracellular iron levels (13). Intestinal HIF-2α is a cellular iron sensor that transcriptionally activates machinery essential for iron absorption in normal physiology and in disease (14). We recently identified that these pathways are integrated; HIF-2α activity is controlled by hepcidin/ferroportin dynamics in the intestine following downstream changes to intestinal epithelial iron concentrations (9). Therefore, in states of normal systemic iron and oxygen, hepatic hepcidin is abundantly produced, and HIF-2α–mediated intestinal iron absorption is restricted. Conversely, during iron demand or systemic hypoxia, hepcidin production is repressed, intestinal ferroportin is stabilized, and intestinal HIF-2α becomes transcriptionally active and up-regulates genes that drive iron absorption. The hepcidin/ferroportin/HIF-2α axis is perturbed in nearly all known iron-related disorders (9, 14). In the context of IDA, a genetic origin was recently discovered that is characterized by hyperactivation of this pathway following mutation to *TMPRSS6* in both mice and humans (15, 16). *TMPRSS6* is a negative regulator of hepcidin

This work was supported by NCI, National Institutes of Health Grant R01CA148828 (to Y. M. S.) and NIDDK, National Institutes of Health Grants R01DK095201 (to Y. M. S.) and F31DK116555 (to A. J. S). The authors declare that they have no conflicts of interest with the contents of this article. The content is solely the responsibility of the authors and does not necessarily represent the official views of the National Institutes of Health.

[1] To whom correspondence should be addressed: Tel.: 734-615-0567; Fax: 734-936-8813; E-mail: shahy@umich.edu.

[2] The abbreviations used are: RBC, red blood cell; IDA, iron deficiency anemia; IRIDA, iron-refractory iron deficiency anemia; Fpn, ferroportin; HCT, hematocrit; MCV, mean corpuscular volume; MCH, mean corpuscular hemoglobin; FTN, ferritin; IRP, iron-regulatory protein; IRE, iron response element; EPO, erythropoietin; LV, left ventricular; qPCR, quantitative PCR; PHD, prolyl hydroxylase domain.

production that, when lost, leads to chronic degradation of ferroportin and progressive and robust IRIDA.

Despite the public health significance of IDA, very little is understood about the kinetics of disease progression and the impact of extreme iron and hypoxic stress on different cell types. Several reports have investigated the role of low iron during development and in the early postnatal period (17, 18); however, these manipulations result in developmental abnormalities and cognitive defects that confound analysis. Further, there are few and poorly characterized genetic models that give rise to severe IDA in mice. Long-term dietary manipulation of iron levels in adult mice can lead to IDA, but this model is variable, and it is difficult to generate a state of end-stage IDA (11). Recent reports have uncovered organ-specific regulatory mechanism of iron homeostasis, particularly in the heart, where a local source of hepcidin is produced to specifically regulate cardiac ferroportin and organ-specific iron homeostasis (19). However, a systematic analysis of cardiac structure, function, and iron and hypoxia sensing during IDA has not been reported. It also remains unclear whether other organs respond similarly through unique mechanisms in IDA.

This paper established an inducible and novel model of progressive end-stage IDA in mice in as little as 3 months. Through temporal *in vivo* deletion of ferroportin exclusively in the intestinal epithelium, this work characterized the kinetics by which IDA progresses following ablation of intestinal iron absorption. In end-stage IDA, tissue-specific hypoxic and iron stress responses were observed; the heart showed relatively little direct hypoxic or iron stress responses despite development of cardiomegaly and cardiac chamber dilation. Echocardiogram analysis in these mice established that IDA decreases the heart rate but with an increased stroke volume, cardiac output, and ejection fraction. Collectively, these data characterized organ-specific stress responses and the cardiac pathologies of IDA in detail. This novel model of IDA can be used to study disease progression and organ-specific responses to iron and hypoxic stress as well as therapies for IRIDA.

Results

Inducible deletion of intestinal epithelial ferroportin in adult mice leads to end-stage iron deficiency anemia

To study the kinetics by which IDA progresses in mice with loss of intestinal iron absorption, *Fpn*-floxed mice were bred to mice that express a tamoxifen-inducible, intestinal epithelium-specific Cre recombinase ($Vil^{CreERT2}$;$Fpn^{fl/fl}$), giving rise, upon tamoxifen treatment, to mice null for ferroportin in the intestinal epithelium ($Fpn^{\Delta IE}$) (9). Adult 2-month-old $Fpn^{fl/fl}$ and $Vil^{CreERT2}$;$Fpn^{fl/fl}$ mice were injected with tamoxifen ($n = 4$, respectively), bled 3 months later to assess blood iron parameters, and then closely monitored until visible phenotypic symptoms of IDA arose (Fig. 1*A*). Six months following tamoxifen injection, $Fpn^{\Delta IE}$ mice began to lose their hair and develop white, translucent paws; all animals were therefore sacrificed at this time point (Fig. 1*B*). The ferroportin protein was still absent in duodenal sections of $Fpn^{\Delta IE}$ mice 6 months following tamoxifen treatment compared with $Fpn^{fl/fl}$ mice (Fig. 1*C*). Complete blood count analysis 3 and 6 months following tamoxifen injection revealed robust progressive IDA; RBC numbers, Hb counts, and hematocrit (HCT) were significantly decreased in $Fpn^{\Delta IE}$ mice compared with $Fpn^{fl/fl}$ littermates, whereas mean corpuscular volume (MCV) and mean corpuscular hemoglobin (MCH) increased from the 3- to 6-month time point, indicating expansion of the reticulocyte pool (Fig. 1*D*). Methylene blue staining confirmed a marked expansion of reticulocytes and an overall decrease in cellularity in $Fpn^{\Delta IE}$ mice (Fig. 1*E*). These data demonstrate that complete ablation of intestinal iron absorption by intestinal epithelial ferroportin deletion in adult mice results in severe IDA in 6 months.

Severe iron deficiency anemia leads to inflammation and necrosis in the liver but spares other organs involved in iron homeostasis

To assess the effect of end-stage IDA on organs involved in maintaining systemic iron homeostasis, the liver, spleen, and duodenum were histologically analyzed by H&E. The spleen was devoid of its red pulp in $Fpn^{\Delta IE}$ mice (Fig. 2*A*). Interestingly, the duodenum was unaffected, potentially explained by the short lifespan of the intestinal epithelium, which is ~3 to 5 days (Fig. 2*A*). Interestingly, the liver exhibited robust morphological damage, including signs of inflammation and necrosis (Fig. 2*A*). To further assess this phenotype, higher-magnification images were taken of liver H&E stains and coupled to picrosirius red staining to reveal collagen deposition and fibrosis. As shown in Fig. 2*B*, $Fpn^{\Delta IE}$ mice displayed marked collagen deposition, particularly surrounding and extending from central veins. Further assessment of the liver revealed inflammatory foci and necrotic areas (Fig. 2*C*). An assessment of inflammatory transcripts indicated that IDA primarily activates *Tgfβ* and *Il6* expression in the liver (Fig. 2*D*). Collectively, these data demonstrate that, among the major players in systemic iron homeostasis, end-stage IDA mostly impacts the liver, resulting in inflammation, necrosis, and activation of Tgfβ and Il6.

End-stage iron deficiency anemia activates a hypoxic transcriptional response in the intestine

IDA starves tissues and cells of both iron and oxygen, which are substrates that control the protein stability of HIF-1α and HIF-2α (20). Intestinal iron absorption requires HIF-2α, the master intestinal transcriptional regulator of apical and basolateral iron transport. We recently showed that the canonical intestinal HIF-2α response is downstream of liver hepcidin kinetics during both iron deficiency and iron overload (9). This axis selectively activates HIF-2α during systemic iron demand, but not HIF-1α, via ferroportin-mediated iron efflux, a response that can be blunted by intracellular iron retention. This work suggests that intestinal epithelial iron levels are the primary stimulus that controls the oxygen-sensitive transcription factor HIF-2α during states of systemic hypoxia. In this study, we sought to investigate the transcriptional response of intestinal hypoxic machinery in end-stage IDA. The duodenal ferroportin (*Fpn*) transcript was significantly reduced in $Fpn^{\Delta IE}$ mice (Fig. 3*A*), confirming efficient recombination 6 months following tamoxifen treatment. Interestingly, activation of iron-absorptive, HIF-2α–specific iron target genes was observed (*Dcytb*, *Dmt1*, and *Ankrd37*), whereas there was no change in

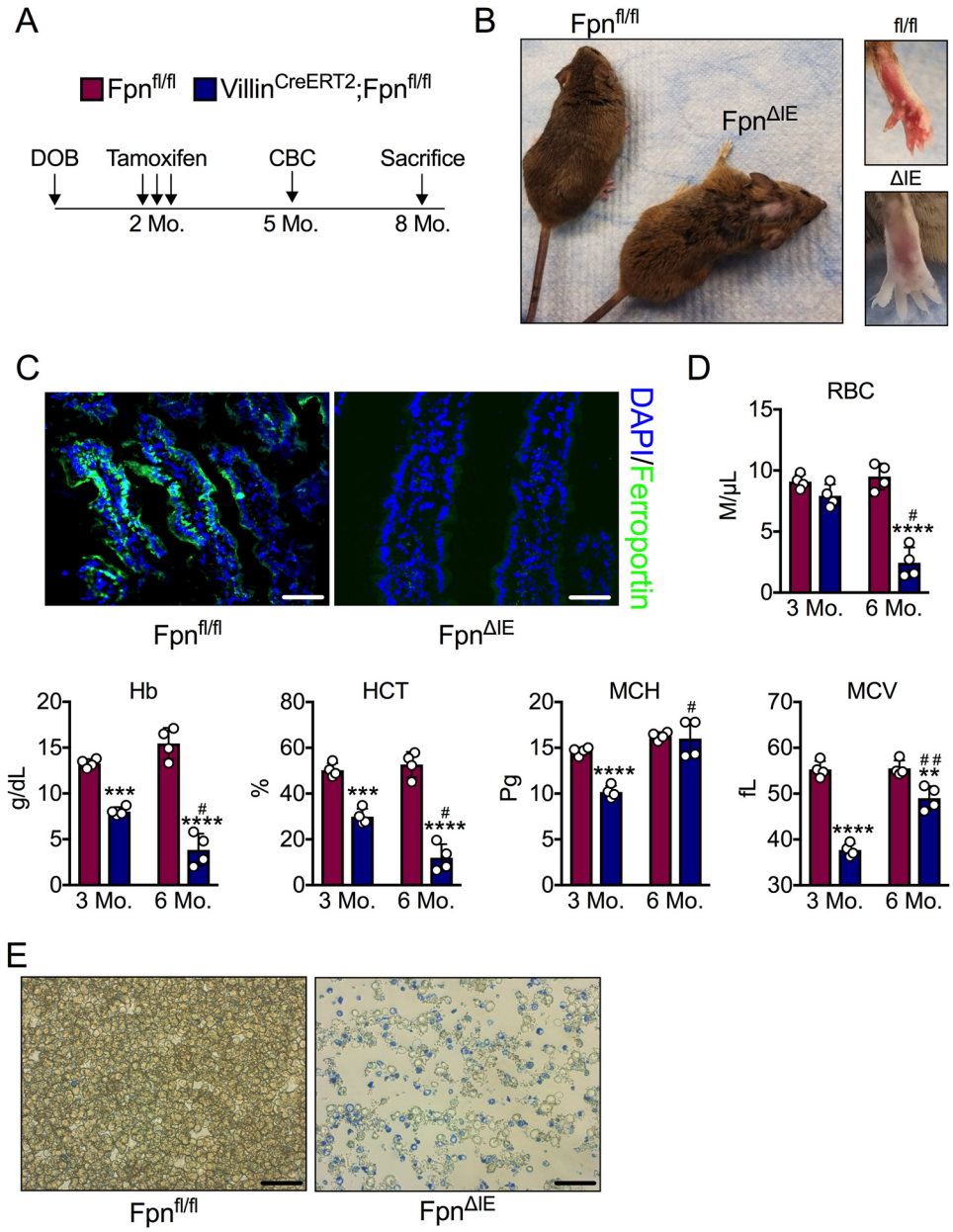

Figure 1. Intestinal epithelial ferroportin deletion in adult mice gives rise to progressive and end-stage iron deficiency anemia. *A*, schematic of the experimental design. *Mo*, month. *DOB*, date of birth; *CBC*, complete blood count. *B*, gross images of $Fpn^{fl/fl}$ and $Fpn^{\Delta IE}$ mice 6 months after tamoxifen administration. *C*, representative ferroportin staining in duodenal sections of $Fpn^{fl/fl}$ and $Fpn^{\Delta IE}$ mice; images at ×40, *scale bars* = 100 μm. *DAPI*, 4′,6-diamidino-2-phenylindole. *D*, analysis of RBCs, Hb, HCT, MCH, and MCV 3 and 6 months following tamoxifen injection. *E*, representative methylene blue staining for reticulocytes; images at ×60, *scale bars* = 150 μm. Mean ± S.E. are plotted. **, $p < 0.01$; ***, $p < 0.001$; ****, $p < 0.0001$ compared between $Fpn^{fl/fl}$ and $Fpn^{\Delta IE}$ cohorts within each time point using two-tailed unpaired *t* test. #, $p < 0.05$; ##, $p < 0.01$ compared between individual $Fpn^{\Delta IE}$ mice at the 3- and 6-month time points using two-tailed paired *t* test.

the expression of the duodenal transferrin receptor (*Tfrc*), an indicator of cellular iron status (Fig. 3*A*). Staining of duodenal sections revealed that the HIF-2α protein was massively stabilized in $Fpn^{\Delta IE}$ mice (Fig. 3*B*). The intracellular iron storage protein ferritin (FTN) was elevated in $Fpn^{\Delta IE}$ mice, confirming iron retention despite systemic IDA (Fig. 3*C*). The HIF-1α–specific target genes *Pdk1*, *Pgk1*, *Bnip3*, and *Ndufa4l2*, which are readouts of intracellular hypoxia, were all elevated (Fig. 3*D*). Last, there was no change in HIF-2α–regulated inflammatory genes (Fig. 3*E*). These data indicate that, despite intestinal epithelial iron retention, end-stage IDA generates a state of intestinal hypoxia that is sufficient to activate HIF-2α–specific iron target genes and HIF-1α–specific target genes but not HIF-2α–regulated inflammatory target genes.

Severe iron deficiency anemia leads to tissue-specific hypoxic and iron stresses that spare the heart

In response to low intracellular oxygen, cells up-regulate anaerobic glycolysis to sustain energy production, a process that is primarily mediated by transcriptional up-regulation of glycolytic genes via HIF-1α activity (21). The transcriptional response to low intracellular iron is regulated primarily by HIF-2α (14). We sought to address the HIF-1α and HIF-2α transcriptional response in peripheral tissues during IDA to

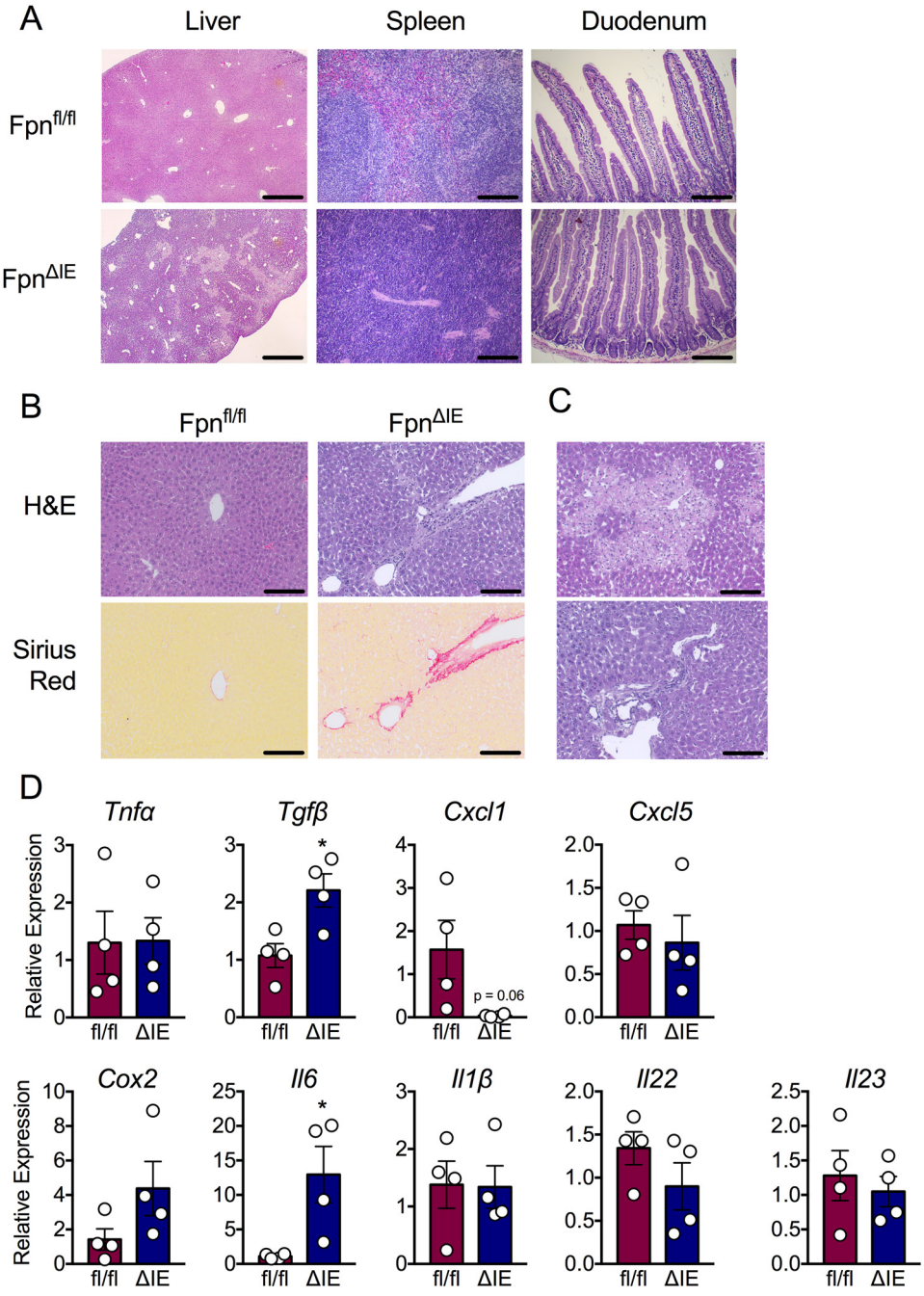

Figure 2. Histological analysis of peripheral organs involved in iron homeostasis reveals inflammation and necrosis in the liver. *A*, representative H&E analysis of liver at ×5 (*scale bars* = 50 μm) and spleen and duodenum at ×20 (*scale bars* = 200 μm) from $Fpn^{fl/fl}$ and $Fpn^{\Delta IE}$ cohorts. *B*, representative H&E and picrosirius red analysis of liver from $Fpn^{fl/fl}$ and $Fpn^{\Delta IE}$ cohorts; images ×20, *scale bars* = 200 μm. *C*, additional representative H&E images of liver from $Fpn^{\Delta IE}$ cohorts; images at ×20, *scale bars* = 200 μm. *D*, qPCR analysis of inflammatory genes in livers of $Fpn^{fl/fl}$ and $Fpn^{\Delta IE}$ cohorts. All data are from mice 6 months post-tamoxifen treatment. Mean ± S.E. are plotted. Significance was determined using two-tailed unpaired *t* test. *, $p < 0.5$ compared between $Fpn^{fl/fl}$ and $Fpn^{\Delta IE}$ cohorts.

assess relative oxygen and iron stress responses. In general, there was significant activation of HIF-1α and HIF-2α target genes in all tissues other than the heart (Fig. 4, *A* and *B*). Of note, expression of erythropoietin (*Epo*), a hormonal signal that increases RBC production, was significantly elevated in the kidneys of $Fpn^{\Delta IE}$ mice, which is a process thought to be repressed during IDA (22–24). Recent literature has demonstrated that the heart maintains iron homeostasis by producing a local source of hepcidin that controls cell-autonomous ferroportin and cardiomyocyte iron levels. We did not observe a significant increase in hepcidin gene (*Hamp*) expression in the heart during IDA (Fig. 4*C*). Collectively, these data demonstrate that IDA engenders hypoxic and iron stress across peripheral tissues other than the heart, which further confirms a unique local mechanism of iron homeostasis in cardiomyocytes.

Iron deficiency anemia leads to cardiac remodeling and pathologies in cardiac structure and function

Patients that suffer from IDA develop cardiac complications (6, 7). Given the unique iron-regulatory mechanisms in the

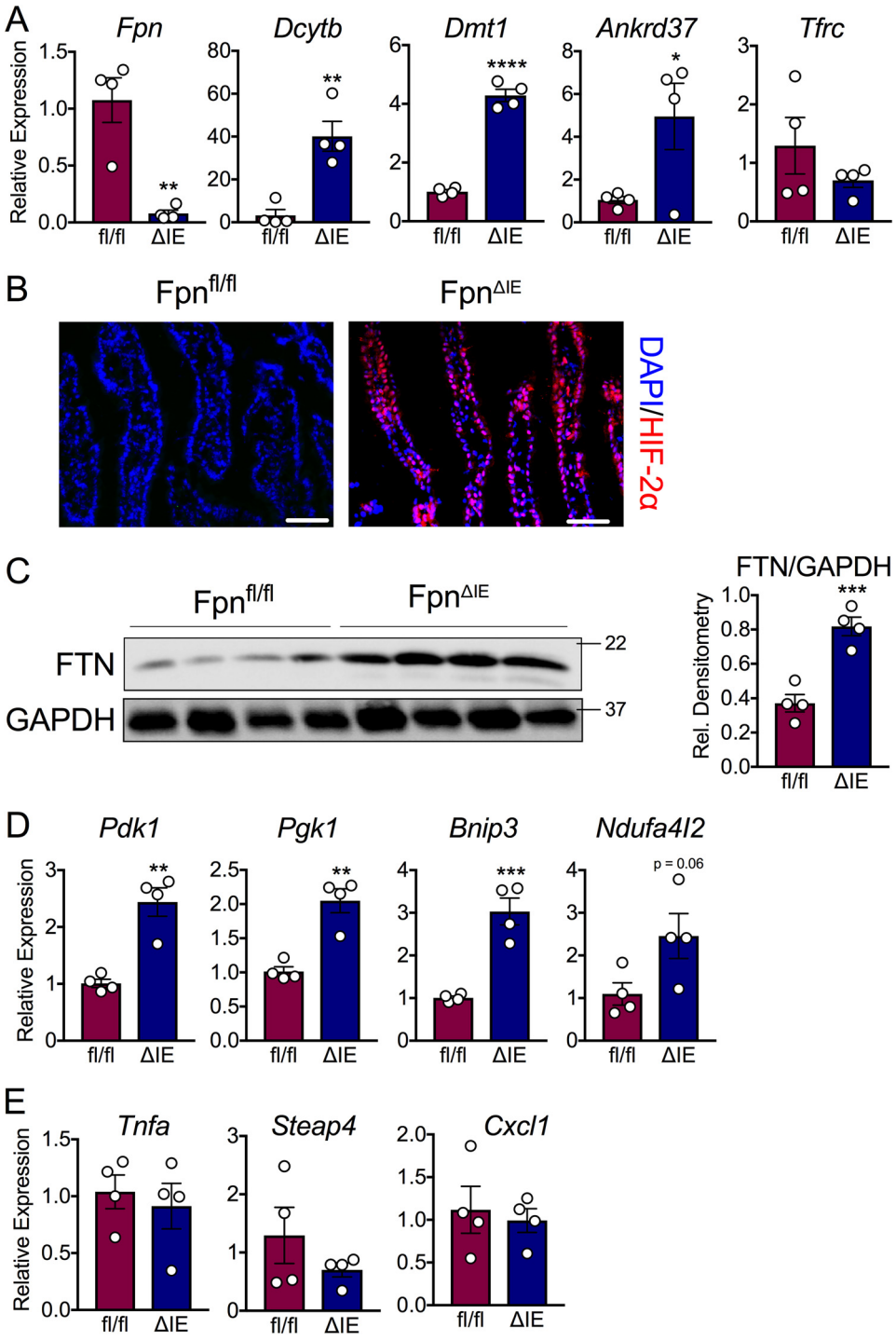

Figure 3. Iron deficiency anemia leads to transcriptional activation of iron and hypoxic target genes in the intestine despite intestinal epithelial iron retention. *A*, qPCR analysis for duodenal HIF-2α–specific and iron-handling transcripts. *B*, representative HIF-2α staining in duodenal sections of $Fpn^{fl/fl}$ and $Fpn^{\Delta IE}$ mice; images at $\times$40, *scale bars* = 100 μm. *DAPI*, 4′,6-diamidino-2-phenylindole. *C*, Western blot analysis and quantification of duodenal FTN abundance. *Rel.*, relative. *D*, qPCR analysis of duodenal HIF-1α–specific transcripts. *E*, qPCR analysis of duodenal HIF-2α–specific and inflammatory transcripts. All data are from mice 6 months post-tamoxifen treatment. Mean ± S.E. are plotted. Significance was determined using two-tailed unpaired *t* test. *, $p < 0.5$; **, $p < 0.01$; ***, $p < 0.001$; ****, $p < 0.0001$ compared between $Fpn^{fl/fl}$ and $Fpn^{\Delta IE}$ cohorts.

heart, we sought to characterize this phenotype by *in vivo* echocardiogram technology 6 months after tamoxifen administration. Forty-eight hours before sacrifice, M-mode echocardiographic analysis revealed increases in septum and posterior wall thickness as well as thickening of papillary muscles in $Fpn^{\Delta IE}$ mice (Fig. 5*A*). Quantitatively, the cardiac structure was tremendously altered, with increases in left ventricular mass, left ventricular volume, interventricular septum, and posterior wall thickness at diastole as well as ascending aorta diameter (Fig. 5*B*). Interestingly, the heart rate was decreased in the $Fpn^{\Delta IE}$ mice despite increases in stroke volume, cardiac output, ejection fraction, and peak velocity in the aorta, confirming disrup-

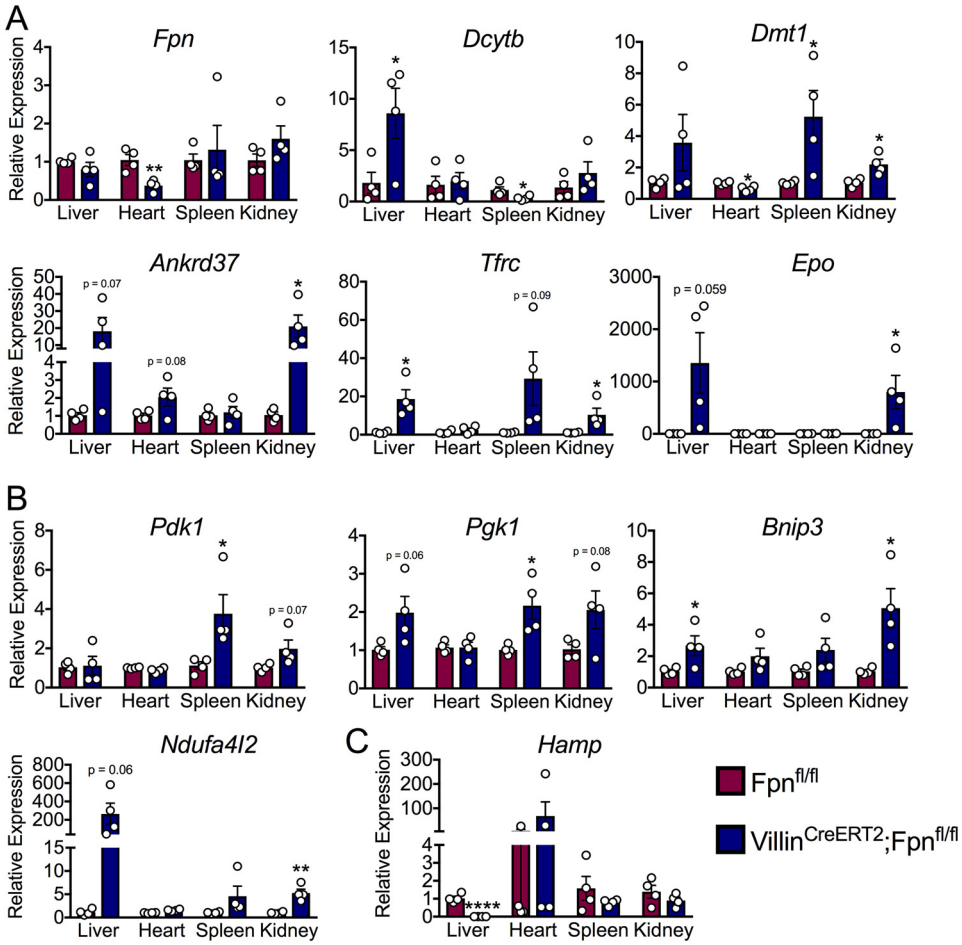

Figure 4. The heart is spared from hypoxic and iron stresses that affect peripheral tissues during iron deficiency anemia. *A*, qPCR analysis of HIF-2α–specific and iron-handling transcripts in the liver, heart, spleen, and kidney. *B*, qPCR analysis of HIF-1α–specific transcripts in the liver, heart, spleen, and kidney. *C*, qPCR analysis of hepcidin (*Hamp*) in the liver, heart, spleen, and kidney. All data are from mice 6 months post-tamoxifen treatment. Mean ± S.E. are plotted. Significance was determined using two-tailed unpaired *t* test. *, $p < 0.5$; **, $p < 0.01$; ****, $p < 0.0001$ compared between $Fpn^{fl/fl}$ and $Fpn^{\Delta IE}$ cohorts within each tissue group.

tion of cardiac function (Fig. 5*C*). Heart iron content was decreased by about 50% despite a quadrupling of left ventricular mass (Fig. 5*D*). Decreases in liver, spleen, and kidney iron content were also observed (Fig. 5*D*). These data, in connection with the data above, demonstrate that IDA does not lead to cardiac hypoxia or iron stress despite tremendous cardiomegaly and perturbation of cardiac function.

Ablation of intestinal epithelial ferroportin in young mice leads to more rapid iron deficiency anemia

To determine whether there was an age effect on the development of IDA following loss of intestinal ferroportin, 2.5-week-old $Fpn^{fl/fl}$ and $Vil^{CreERT2}$;$Fpn^{fl/fl}$ mice were injected with tamoxifen and monitored closely (Fig. 6*A*). By 3 months following treatment, $Fpn^{\Delta IE}$ mice began to display similar phenotypic changes to the aforementioned adult cohort (*e.g.* hair loss, white paws, etc.) and were euthanized. The ferroportin protein was absent in duodenal sections of $Fpn^{\Delta IE}$ mice (Fig. 6*B*). Furthermore, the ferroportin transcript was significantly decreased in this $Fpn^{\Delta IE}$ cohort (Fig. 6*C*). Complete blood count analysis revealed robust IDA; RBC, Hb, HCT, MCH, and MCV were all significantly decreased in $Fpn^{\Delta IE}$ mice compared with $Fpn^{fl/fl}$ littermates, to the same extent as adult mice 6 months following treatment (Fig. 6*D*). Furthermore, heart mass normalized to tibia length was increased already 3 months after tamoxifen injection, indicating cardiac hypertrophy (Fig. 6*E*). These data demonstrate that young mice progress to IDA more rapidly by intestinal ferroportin ablation than adult mice and that this genetic model of severe IDA with cardiomegaly can be made more rapid by treating young $Vil^{CreERT2}$;$Fpn^{fl/fl}$ mice with tamoxifen.

Discussion

A constant influx of postnatal intestinal iron is critical to maintain intracellular iron concentrations for metabolism and erythropoiesis for systemic oxygen transport in mammals. However, iron deficiency remains the most common nutrient deficiency in humans, affecting nearly 2 billion people worldwide (4). Of these, over 1 billion people suffer from IDA, a state of iron insufficiency that limits the production of RBCs and results in systemic tissue hypoxia and intracellular iron stress (2). Few model systems exist to study the kinetics of IDA and the effect of extreme iron and oxygen stress on peripheral tissues. This work demonstrates a temporal model of severe IDA in mice via tamoxifen-inducible ablation of ferroportin in the intestinal epithelium. In as little as 3 months, severe end-stage

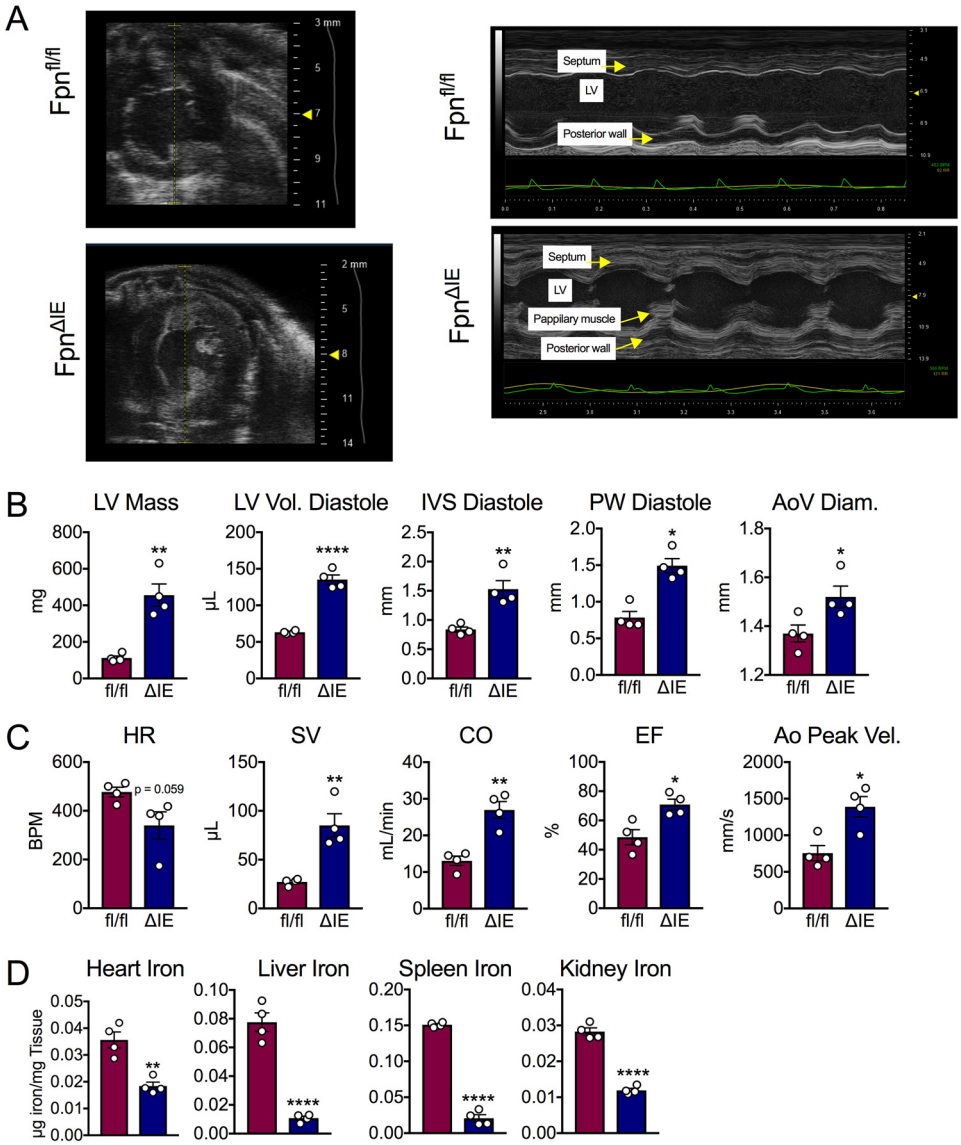

Figure 5. Echocardiogram analysis of iron deficiency anemia reveals cardiomegaly and disruption of cardiac function. *A*, M-mode images from echocardiogram analysis in $Fpn^{fl/fl}$ and $Fpn^{\Delta IE}$ mice with end-stage iron deficiency anemia. *B*, quantification of cardiac structure parameters: left ventricular mass (*LV Mass*), left ventricular volume at diastole (*LV Vol. Diastole*), interventricular septum width at diastole (*IVS Diastole*), posterior wall thickness at diastole (*PW Diastole*), and ascending aorta diameter (*AoV Diam.*). *C*, quantification of cardiac function parameters: heart rate (*HR*), stroke volume (*SV*), cardiac output (*CO*), ejection fraction (*EF*), and aorta velocity peak gradient (*Ao Peak Vel.*). *D*, heart, liver, spleen, and kidney iron content. All data are from mice 6 months post-tamoxifen treatment. Mean ± S.E. are plotted. Significance was determined using two-tailed unpaired *t* test. *, $p < 0.5$; **, $p < 0.01$; ****, $p < 0.0001$ compared between $Fpn^{fl/fl}$ and $Fpn^{\Delta IE}$ cohorts

IDA was observed when 2.5-week-old $Vil^{CreERT2}$;$Fpn^{fl/fl}$ mice were treated with tamoxifen. We discovered tissue-specific activation of hypoxic and iron transcriptional stress responses where the heart is largely spared compared with other peripheral organs. This transcriptional phenomenon was observed despite the quadrupling of left ventricular mass, significant increases in cardiac output, and development of cardiomegaly, as revealed by *in vivo* echocardiogram. We also demonstrate that severe IDA can activate the HIF-2α iron-absorptive transcriptional program in the intestine despite a surplus of intracellular iron. Collectively, this work reveals a robust and reliable model to study IDA, tissue-specific responses to iron and oxygen stress, and the mechanisms of cardiac remodeling in iron-related disorders.

Previous models that give rise to IDA in mice have utilized strategies of dietary iron manipulation or genetic deletion of iron handling in the embryo (6, 11, 17, 18). However, mice are extremely resistant to IDA when placed on iron-deficient diets (9, 11). This can be explained, at least in part, by iron contamination in proprietary diets. The ubiquitous nature of iron-containing proteins complicates the ability to remove iron from these diets, leaving behind sufficient iron levels to maintain systemic iron homeostasis for extended periods of time. Genetic models that manipulate intestinal iron absorption have relied on embryonic knockout strategies (18, 25). These models dramatically disrupt embryonic and postnatal development, as disruption to iron homeostasis early in life can affect organ development and overall cognitive function (17). Our present

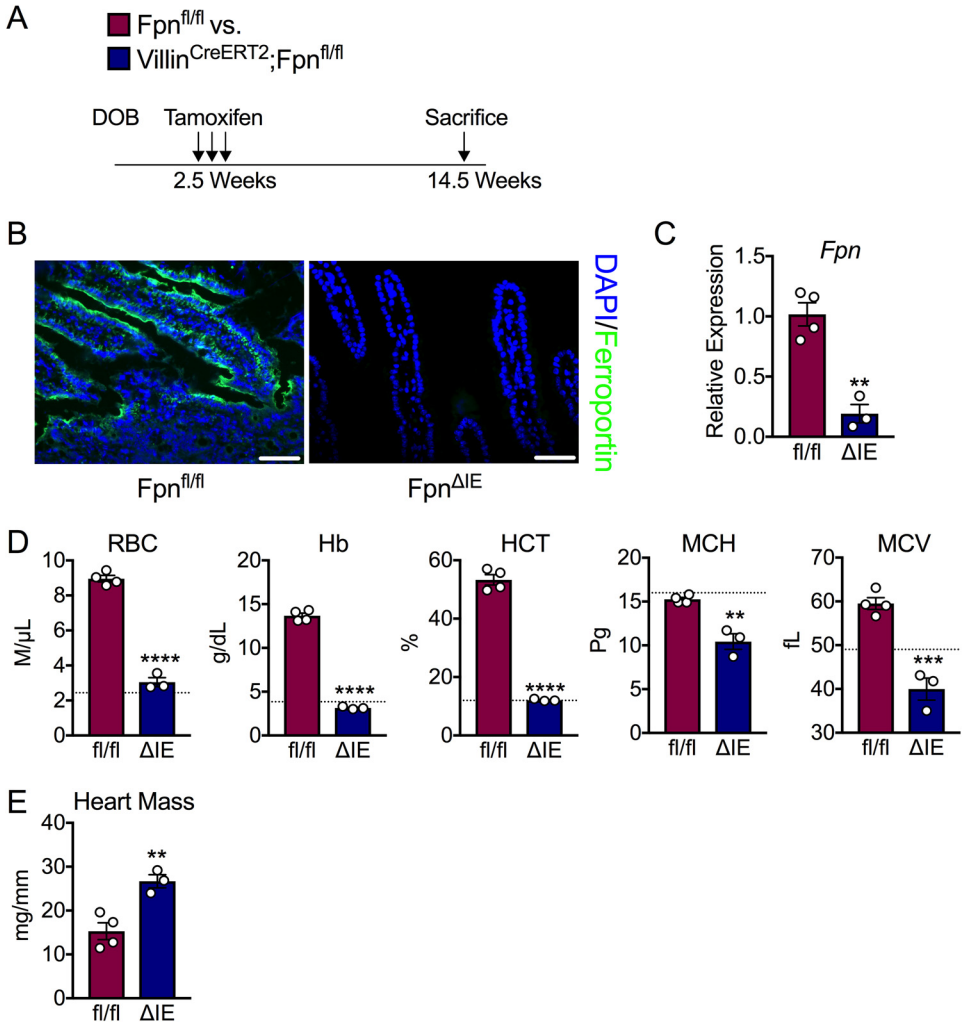

Figure 6. End-stage iron deficiency anemia develops more rapidly when induced in young mice. *A*, schematic of the experimental design. *DOB*, date of birth. *B*, representative ferroportin staining in duodenal sections of $Fpn^{fl/fl}$ and $Fpn^{\Delta IE}$ mice; images at ×40, *scale bars* = 100 μm. *C*, qPCR analysis of the duodenal *Fpn* transcript in $Fpn^{fl/fl}$ and $Fpn^{\Delta IE}$ mice. *D*, analysis of RBCs, Hb, HCT, MCH, and MCV. The *dashed lines* indicate 6-month values observed in the experiment with $Fpn^{\Delta IE}$ adult mice reported in Fig. 1. *E*, heart mass normalized to tibia length. All data are from mice 3 months post-tamoxifen treatment. Mean ± S.E. are plotted. Significance was determined using two-tailed unpaired *t* test. **, $p < 0.01$; ***, $p < 0.001$; ****, $p < 0.0001$ compared between $Fpn^{fl/fl}$ and $Fpn^{\Delta IE}$ cohorts.

model of IDA allows postnatal development and the establishment of proper iron homeostasis before inducing a disease state. Surprisingly, mouse survival appeared to be unaffected despite mean hemoglobin levels of less than 5 g/dl and mean hematocrits of less than 12%. The lowest observed hematocrit was 6.5%. Previous experiments in anesthetized animals with isovolumic anemia have shown that oxygen delivery can be maintained to approximately similar Hb concentrations (3–5 g/dl) and hematocrits (10%–15%), but organ function starts to decline near these values and is correlated with development of lactic acidosis (26). Furthermore, the progressive nature of this genetic model allows temporal characterization of IDA in ways never executed before. This model is limited, however, because it recapitulates IRIDA, a rare phenotype of IDA that is refractory to oral iron supplementation because of the inability to absorb intestinal iron. Future work will need to carefully describe IDA progression and more clearly define the mechanisms behind disparate intracellular stress responses in peripheral tissues.

In addition to the hepcidin/ferroportin/HIF-2α axis that regulates systemic iron homeostasis, there exists a ubiquitous cell-autonomous mechanism of intracellular iron sensing and regulation via iron-regulatory protein (IRP) and iron response element (IRE) machinery. This system controls cellular iron homeostasis by modulating the translation of mRNAs involved in iron handling via binding of IRPs with IREs in the 5′ or 3′ UTR of these transcripts. Erythropoietin (EPO), an endocrine hormone produced by the kidney to drive RBC production in the bone marrow, is a classical HIF-2α target gene regulated by systemic hypoxia (24, 27). HIF-2α contains a 5′ UTR IRE that is responsible for translational inhibition during states of iron deficiency (22–24). This IRP/IRE interaction is thought to serve as a molecular brake on HIF-2α–mediated kidney EPO expression to restrict RBC production when iron levels are limited for hemoglobin synthesis. Surprisingly, we found in this work that the *Epo* transcript is induced 1000-fold despite severe kidney iron deficiency in IDA. This finding may indicate that the IRP/IRE system is an insufficient mechanism to dampen HIF-2α in

the kidney during the severe disease state of IDA. Moreover, high EPO production in IDA is likely a pathological feature where red blood cell production is continually attempted despite insufficient circulating iron levels. This finding may explain the expansion of reticulocytes we observed. In addition to IRE/IRP machinery, HIF-2α is also regulated at the posttranscriptional level by PHD enzymes, where intracellular iron deficiency limits PHD enzyme activity to stabilize the HIF-2α protein (9). It is therefore possible that a hepcidin/ferroportin/PHD axis may exist in EPO-producing cells in the kidney, similar to the intestine, where the hepcidin/ferroportin/PHD induction of HIF-2α outweighs the IRP/IRE break on HIF-2α in contexts when both pathways are active. In the intestine, the dominance of the hepcidin/ferroportin/PHD axis over IRP/IRE machinery enables HIF-2α protein stabilization and an increase in iron absorption during states of iron deficiency. However, in the kidney during IDA, the interplay between these pathways appears to be pathological, given the inappropriate, sustained, and paradoxical production of EPO. More work will need to be done to understand the complete molecular mechanisms of *Epo* expression during normal physiology and in disease states such as IDA.

Transcriptional stress responses to states of low intracellular oxygen are mediated by the family of hypoxia-inducible factors; namely, HIF-1α and HIF-2α. These transcription factors activate unique and overlapping target genes to up-regulate anaerobic glycolysis and modulate cellular metabolism to survive in low oxygen environments (14, 20, 21). Our laboratory, among others, has shown that HIF-2α, but not HIF-1α, is a direct cellular iron sensor (10, 12). More recently, we revealed that intestinal HIF-2α is primarily regulated by intracellular iron levels during states of systemic iron demand; the canonical and physiological HIF-2α response can be blunted by a state of intracellular iron excess (9). Interestingly, we show in this work that the intestinal HIF-2α iron-absorptive transcriptional program is active during severe IDA despite excess intracellular iron following ferroportin ablation. This finding suggests that, although intestinal HIF-2α is mainly responsive to intracellular iron levels in physiological iron demand, HIF-2α maintains an oxygen-sensing capacity during severe tissue hypoxia in IDA. Interestingly, HIF-2α transcriptional targets involved in inflammation were not active despite activation of iron-absorptive genes. This finding is in line with recent work showing that HIF-2α functions with cofactors and other transcriptional partners to regulate subsets of target genes when the protein is stabilized (28, 29). Future work will need to define how specific HIF target genes are regulated during unique environmental ques as well as the relative contribution of HIF-2α oxygen and iron sensing in different cells and tissues.

Cardiac structure and function are perturbed in iron-related disorders, including iron deficiency, iron overload, and anemia. In IDA in humans, the heart undergoes massive cardiac hypertrophy and remodeling to increase cardiac output and prolong survival when systemic oxygen transport becomes limited (30, 31). A recent study comparing genetic models of sickle cell anemia with diet-induced IDA in adult mice showed that, after 3 months of anemia (5–9 g/dl Hb with a IDA target of 7.5 g/dl Hb), both models develop a high-output functional state in the heart (32). However, although sickle cell anemia produced more severe restrictive cardiomyopathy with fibrotic remodeling, this study reported that 3 months of IDA beginning at 5 months of age failed to produce significant cardiac hypertrophy (32). This is consistent with our findings of a more slowly progressing IDA phenotype in adult mice and suggests that hemoglobin concentrations of less than 5 g/dl and hematocrits of less than 15% in IDA are required to induce significant cardiac hypertrophy. Interestingly, the cardiac hypertrophy in IDA can be explained, at least in part, simply by decreases in cardiac iron stores because genetic disruption of serum uptake of iron exclusively in cardiomyocytes leads to cardiac hypertrophy (33). Using *in vivo* echocardiograms, in this work we detail the structural and functional changes that occur in the heart during severe IDA. We observed structural changes that include quadrupling of left ventricular mass and increases in left ventricular volume and posterior wall thickness at diastole. We also observed increases in cardiac output and stroke volume despite a decrease in heart rate and total heart iron content. Interestingly, despite these pathophysiological changes, the heart was largely spared from transcriptional stress responses downstream of HIF that would demonstrate tissue hypoxia and iron stress. Recent literature has revealed that cardiomyocytes rely on cell-autonomous mechanisms to control iron homeostasis in the heart that are distinct from systemic mechanisms of iron homeostasis (19). Although normal mice do not normally show lower arterial blood oxygen saturation or heart rate under the 1%–1.5% isoflurane conditions used here for the cardiac function studies (34–36), we cannot rule out that IDA mice are more susceptible to subtle effects of isoflurane on arterial blood oxygen saturation. We note that the mice in this work were maintained on 1%–1.5% isoflurane delivered in 100% oxygen carrier gas even though room air is sufficient to maintain arterial oxygen saturation in isoflurane-anesthetized WT mice (35). Taken together, these data may suggest that cell-autonomous mechanisms of cardiac iron handling are sufficient to prevent overt iron and oxygen stress during IDA. Moreover, it is possible that the heart is somehow spared by peripheral organs and that serum iron and oxygen are redirected to the heart during stress. Future work will need to identify the signaling pathways that mediate the robust cardiac remodeling that is observed in IDA as well as the complete molecular mechanisms of cardiac iron homeostasis that prevent hypoxic and iron transcriptional stress responses.

In conclusion, our work demonstrates a novel, robust, and inducible model of IDA in mice. We provide new insights into the molecular mechanisms of HIF signaling and IRP/IRE kinetics. We also characterize the cardiac changes of IDA and unveil unique tissue-specific transcriptional stress responses across peripheral tissues during hypoxic and iron stress.

Experimental procedures

Animals and treatments

Vil^{CreERT2};*Fpn*$^{fl/fl}$ mice were described previously (9). Analysis began on mice that were either 2.5 weeks or 8 weeks of age, as indicated. Mice were injected with tamoxifen (Sigma-Aldrich, St. Louis, MO) at 100 mg/kg of body weight i.p. for three

consecutive days to ensure Cre-mediated recombination. All mice were fed with standard chow (Research Diets, New Brunswick, NJ) unless indicated as being fed a purified AIN-93G iron-replete (350 ppm) or low-iron (<5 ppm) diet (Dyets, Bethlehem, PA). For intestinal protein and RNA analysis, duodenal epithelial scrapes were performed; the intestine was opened flat, and a microscope slide was used to scrape and collect epithelial cells, leaving behind the submucosa. All mice were housed at the Unit for Laboratory Animal Management at the University of Michigan. All animal studies were carried out in accordance with Institute of Laboratory Animal Resources guidelines and approved by the University Committee on the Use and Care of Animals at the University of Michigan (protocol PRO00008292).

Hematological and iron analysis

The Unit for Laboratory Animal Medicine Pathology Core at the University of Michigan performed complete blood count analysis. Nonheme iron was quantified as described previously (9). Briefly, tissues were homogenized at 100 μl/10 mg in deionized water and incubated with an equal volume of an acid digestion solution (*i.e.* 1 M HCl and 10% TCA; Sigma-Aldrich) for 1 h at 95 °C. Homogenates were spun at full speed for 10 min, and 50 μl of supernatant was mixed with 50 μl of a substrate containing 1:1 1 mM ferrozine:3 M sodium acetate and 1% mercaptoacetic acid. Reactions were read at 562 nm.

Quantitative RT-PCR

mRNA was extracted using TRIzol (Thermo Scientific, Waltham, MA) according to the manufacturer's instructions. mRNA was measured by real-time RT-PCR (Life Technologies) using SYBR Green Mix (Alkali Scientific, Ft. Lauderdale, FL). Primers are listed in Table 1. Quantification cycle values were normalized to β-actin and expressed as -fold change.

Western blotting

Whole-cell lysates were prepared in RIPA buffer as described previously (9). In brief, lysates were separated by SDS-PAGE, transferred to a nitrocellulose membrane, and probed overnight at 4 °C with antibodies for FTN (Cell Signaling, Danvers, MA) or GAPDH (Santa Cruz, Dallas, TX). Secondary antibodies were purchased from Santa Cruz Biotechnology (Dallas, TX), and membranes were developed using enhanced chemiluminescence substrate (Thermo Scientific).

Histological and immunohistochemical analysis

Bright-field histologic analysis was performed on H&E- and picrosirius red–stained, formalin-fixed, paraffin-embedded sections using reagents from Sigma-Aldrich. In brief, for Picrosirius red staining, slides were deparaffinized and incubated with picrosirius red for 1 h and washed with an acid solution containing 0.5% acetic acid. Immunohistochemical analysis was performed on frozen sections following fixation with 10% buffered formalin and blocking with 5% goat serum using antibodies against ferroportin (MTP11-A, ADI, San Antonio, TX) or HIF-2α (100–122, Novus, St. Louis, MO). For reticulocyte analysis, a 1% methylene blue (Sigma) solution was mixed with equal volumes of blood, incubated at room temperature for 10 min, and then smeared onto a microscope slide.

Table 1
qPCR primers

Gene	Primer sequence
Dcytb F	CATCCTCGCCATCATCTC
Dcytb R	GGCATTGCCTCCATTTAGCTG
DMT1 F	TTGGCAATCATTGGTTCTGA
DMT1 R	CTTCCGCAAGCCATATTTGT
Ferroportin F	ATGGGAACTGTGGCCTTCAC
Ferroportin R	TCCAGGCATGAATACGGAGA
Ankrd37 F	CGGCCTTGCGTGCTTT
Ankrd37 R	TGGTTGAGGTCAGCACCTGTT
Transferrin receptor F	CAGTCCAGCTGGCAAAGATT
Transferrin receptor R	GTCCAGTGTGGGAACAGGTC
PDK1 F	TTACTCAGTGGAACACCGCC
PDK1 R	GTTTATCCCCCGATTCAGGT
PGK1 F	CAAATTTGATGAGAATGCCAAGACT
PGK1 R	TTCTTGCTGCTCTCAGTACCACA
Bnip3 F	TGAAGTGCAGTTCTACCCAGG
Bnip3 R	CCTGTCGCAGTTGGGTTC
Ndufa4I2 F	AGTCTAGGGACCCGCTTCTAC
Ndufa4I2 R	TGTACTGGTCATTGGGACTCA
STEAP4 F	GGAAACTCATCTGCATGTGCT
STEAP4 R	CTAGAAGGCAGAGCCCACC
CXCL1 F	TCTCCGTTACTTGGGGACAC
CXCL1 R	CCACACTCAAGAATGGTCGC
Erythropoietin F	CATCTGCGACAGTCGAGTTCTG
Erythropoietin R	CACAACCCATCGTGACATTTTC
Hamp1 F	CTATCTCCATCAACAGATGAGACAGA
Hamp1 R	AACAGATACCACACTGGGAA
Tnfα F	AGGGTCTGGGCCATAGAACT
Tnfα R	CCACCACGCTCTTCTGTCTAC
Tgfβ F	CAACCCAGGTCCTTCCTAAA
Tgfβ R	GGAGAGCCCTGGATACCAAC
CXCL5 F	TGCATTCCGCTTAGCTTTCT
CXCL5 R	CAGAAGGAGGTCTGTCTGGA
Cox 2 F	GGCGCAGTTTATGTTGTCTGT
Cox 2 R	CAAGACAGATCATAAGCGAGGA
Il6 F	ACCAGAGGAAATTTTCAATAGGC
Il6 R	TGATGCACTTGCAGAAAACA
Il1β F	AAGAGCTTCAGGCAGGCAGTATCA
Il1β R	TGCAGCTGTCTAGGAACGTCA
Il22 F	TCGCCTTGATCTCTCCACTC
Il22 R	GCTCAGCTCCTGTCACATCA
IL23 F	GCTCCCCTTTGAAGATGTCA
Il23 R	GACCCACAAGGACTCAAGGA

Echocardiogram analysis

Echocardiography was performed as described previously (37). Briefly, induction of anesthesia was performed in an enclosed container filled with 6% isoflurane. After induction, the mice were placed on a warming pad to maintain body temperature. 1%–1.5% isoflurane was supplied via a nose cone to maintain a surgical plane of anesthesia. In all studies, the isoflurane was delivered with 100% oxygen carrier gas, and the mice were anesthetized for less than 30 min in total to collect functional data and limit any isoflurane effect that may confound experimental results. The hair was removed from the upper abdominal and thoracic area with depilatory cream. ECG was monitored via noninvasive resting ECG electrodes. Transthoracic echocardiography was performed in the supine or left lateral position. Two-dimensional, M-mode, Doppler and tissue Doppler echocardiography images were recorded using a Visual Sonics Vevo 2100 high-resolution *in vivo* microimaging system with a MS 550D transducer that has a center frequency of 40 MHz and a bandwidth of 22–55 MHz. We measured the LV ejection fraction from the two-dimensional long axis view. We measured systolic and diastolic dimensions and wall thickness by M-mode in the parasternal short axis view at the level of the

papillary muscles. Fractional shortening and ejection fraction were also calculated from the M-mode parasternal short axis view. Diastolic function was assessed by conventional pulsed-wave spectral Doppler analysis of mitral valve inflow patterns (early (E) and late (A) filling waves). Doppler tissue imaging was used to measure the early (Ea) diastolic tissue velocities of the septal annulus of the mitral valve in the apical 4-chamber view.

Statistics

Results are expressed as mean ± S.E. Significance between two groups was calculated by unpaired *t* test. Prism 7.0 software (GraphPad Software, La Jolla, CA) was used to conduct analyses.

Author contributions—A. J. S. and Y. M. S. conceptualization; A. J. S. data curation; A. J. S., K. C.-B., and D. E. M. formal analysis; A. J. S. writing-original draft; A. J. S., D. E. M., and Y. M. S. writing-review and editing; K. C.-B. and D. E. M. methodology; Y. M. S. funding acquisition; Y. M. S. project administration.

References

1. Drakesmith, H., Nemeth, E., and Ganz, T. (2015) Ironing out ferroportin. *Cell Metab.* **22,** 777–787 CrossRef Medline
2. McLean, E., Cogswell, M., Egli, I., Wojdyla, D., and de Benoist, B. (2009) Worldwide prevalence of anaemia, WHO Vitamin and Mineral Nutrition Information System. 1993–2005. *Public Health Nutr.* **12,** 444–454 CrossRef Medline
3. Muckenthaler, M. U., Rivella, S., Hentze, M. W., and Galy, B. (2017) A red carpet for iron metabolism. *Cell* **168,** 344–361 CrossRef Medline
4. Camaschella, C. (2015) Iron-deficiency anemia. *N. Engl. J. Med.* **372,** 1832–1843 CrossRef Medline
5. Heeney, M. M., and Finberg, K. E. (2014) Iron-refractory iron deficiency anemia (IRIDA). *Hematol. Oncol. Clin. North Am.* **28,** 637–652 CrossRef Medline
6. Chung, Y. J., Luo, A., Park, K. C., Loonat, A. A., Lakhal-Littleton, S., Robbins, P. A., and Swietach, P. (2019) Iron-deficiency anemia reduces cardiac contraction by downregulating RyR2 channels and suppressing SERCA pump activity. *JCI Insight* **4,** 125618 Medline
7. Sutil-Vega, M., Rizzo, M., and Martínez-Rubio, A. (2019) Anemia and iron deficiency in heart failure: a review of echocardiographic features. *Echocardiography* **36,** 585–594 CrossRef Medline
8. Anderson, E. R., Xue, X., and Shah, Y. M. (2011) Intestinal hypoxia-inducible factor-2α (HIF-2α) is critical for efficient erythropoiesis. *J. Biol. Chem.* **286,** 19533–19540 CrossRef Medline
9. Schwartz, A. J., Das, N. K., Ramakrishnan, S. K., Jain, C., Jurkovic, M. T., Wu, J., Nemeth, E., Lakhal-Littleton, S., Colacino, J. A., and Shah, Y. M. (2019) Hepatic hepcidin/intestinal HIF-2α axis maintains iron absorption during iron deficiency and overload. *J. Clin. Invest.* **129,** 336–348 Medline
10. Shah, Y. M., Matsubara, T., Ito, S., Yim, S. H., and Gonzalez, F. J. (2009) Intestinal hypoxia-inducible transcription factors are essential for iron absorption following iron deficiency. *Cell Metab.* **9,** 152–164 CrossRef Medline
11. Taylor, M., Qu, A., Anderson, E. R., Matsubara, T., Martin, A., Gonzalez, F. J., and Shah, Y. M. (2011) Hypoxia-inducible factor-2α mediates the adaptive increase of intestinal ferroportin during iron deficiency in mice. *Gastroenterology* **140,** 2044–2055 CrossRef Medline
12. Mastrogiannaki, M., Matak, P., Keith, B., Simon, M. C., Vaulont, S., and Peyssonnaux, C. (2009) HIF-2α, but not HIF-1α, promotes iron absorption in mice. *J. Clin. Invest.* **119,** 1159–1166 CrossRef Medline
13. Nemeth, E., Tuttle, M. S., Powelson, J., Vaughn, M. B., Donovan, A., Ward, D. M., Ganz, T., and Kaplan, J. (2004) Hepcidin regulates cellular iron efflux by binding to ferroportin and inducing its internalization. *Science* **306,** 2090–2093 CrossRef Medline
14. Shah, Y. M., and Xie, L. (2014) Hypoxia-inducible factors link iron homeostasis and erythropoiesis. *Gastroenterology* **146,** 630–642 CrossRef Medline
15. Finberg, K. E., Heeney, M. M., Campagna, D. R., Aydinok, Y., Pearson, H. A., Hartman, K. R., Mayo, M. M., Samuel, S. M., Strouse, J. J., Markianos, K., Andrews, N. C., and Fleming, M. D. (2008) Mutations in TMPRSS6 cause iron-refractory iron deficiency anemia (IRIDA). *Nat. Genet.* **40,** 569–571 CrossRef Medline
16. Guo, S., Casu, C., Gardenghi, S., Booten, S., Aghajan, M., Peralta, R., Watt, A., Freier, S., Monia, B. P., and Rivella, S. (2013) Reducing TMPRSS6 ameliorates hemochromatosis and β-thalassemia in mice. *J. Clin. Invest.* **123,** 1531–1541 CrossRef Medline
17. Ramakrishnan, S. K., Anderson, E. R., Martin, A., Centofanti, B., and Shah, Y. M. (2015) Maternal intestinal HIF-2α is necessary for sensing iron demands of lactation in mice. *Proc. Natl. Acad. Sci. U.S.A.* **112,** E3738–E3747 CrossRef Medline
18. Donovan, A., Lima, C. A., Pinkus, J. L., Pinkus, G. S., Zon, L. I., Robine, S., and Andrews, N. C. (2005) The iron exporter ferroportin/Slc40a1 is essential for iron homeostasis. *Cell Metab.* **1,** 191–200 CrossRef Medline
19. Lakhal-Littleton, S., Wolna, M., Chung, Y. J., Christian, H. C., Heather, L. C., Brescia, M., Ball, V., Diaz, R., Santos, A., Biggs, D., Clarke, K., Davies, B., and Robbins, P. A. (2016) An essential cell-autonomous role for hepcidin in cardiac iron homeostasis. *Elife* **5,** e19804 CrossRef Medline
20. Keith, B., Johnson, R. S., and Simon, M. C. (2011) HIF1α and HIF2α: sibling rivalry in hypoxic tumour growth and progression. *Nat. Rev. Cancer* **12,** 9–22 CrossRef Medline
21. Semenza, G. L. (2013) HIF-1 mediates metabolic responses to intratumoral hypoxia and oncogenic mutations. *J. Clin. Invest.* **123,** 3664–3671 CrossRef Medline
22. Sanchez, M., Galy, B., Muckenthaler, M. U., and Hentze, M. W. (2007) Iron-regulatory proteins limit hypoxia-inducible factor-2α expression in iron deficiency. *Nat. Struct. Mol. Biol.* **14,** 420–426 CrossRef Medline
23. Anderson, S. A., Nizzi, C. P., Chang, Y. I., Deck, K. M., Schmidt, P. J., Galy, B., Damnernsawad, A., Broman, A. T., Kendziorski, C., Hentze, M. W., Fleming, M. D., Zhang, J., and Eisenstein, R. S. (2013) The IRP1-HIF-2α axis coordinates iron and oxygen sensing with erythropoiesis and iron absorption. *Cell Metab.* **17,** 282–290 CrossRef Medline
24. Wilkinson, N., and Pantopoulos, K. (2013) IRP1 regulates erythropoiesis and systemic iron homeostasis by controlling HIF2α mRNA translation. *Blood* **122,** 1658–1668 CrossRef Medline
25. Chen, A. C., Donovan, A., Ned-Sykes, R., and Andrews, N. C. (2015) Noncanonical role of transferrin receptor 1 is essential for intestinal homeostasis. *Proc. Natl. Acad. Sci. U.S.A.* **112,** 11714–11719 CrossRef Medline
26. Viele, M. K., and Weiskopf, R. B. (1994) What can we learn about the need for transfusion from patients who refuse blood? The experience with Jehovah's Witnesses. *Transfusion* **34,** 396–401 CrossRef Medline
27. Wang, G. L., and Semenza, G. L. (1993) General involvement of hypoxia-inducible factor 1 in transcriptional response to hypoxia. *Proc. Natl. Acad. Sci. U.S.A.* **90,** 4304–4308 CrossRef Medline
28. Ma, X., Das, N. K., Castillo, C., Gourani, A., Perekatt, A. O., Verzi, M. P., and Shah, Y. M. (2019) SMAD family member 3 (SMAD3) and SMAD4 repress HIF2α-dependent iron-regulatory genes. *J. Biol. Chem.* **294,** 3974–3986 CrossRef Medline
29. Xue, X., Ramakrishnan, S., Anderson, E., Taylor, M., Zimmermann, E. M., Spence, J. R., Huang, S., Greenson, J. K., and Shah, Y. M. (2013) Endothelial PAS domain protein 1 activates the inflammatory response in the intestinal epithelium to promote colitis in mice. *Gastroenterology* **145,** 831–841 CrossRef Medline
30. Hayashi, R., Ogawa, S., Watanabe, Z., and Yamamoto, M. (1999) Cardiovascular function before and after iron therapy by echocardiography in patients with iron deficiency anemia. *Pediatr. Int.* **41,** 13–17 CrossRef Medline
31. Zhou, Q., Shen, J., Liu, Y., Luo, R., Tan, B., and Li, G. (2017) Assessment of left ventricular systolic function in patients with iron deficiency anemia by three-dimensional speckle-tracking echocardiography. *Anatol. J. Cardiol.* **18,** 194–199 Medline
32. Bakeer, N., James, J., Roy, S., Wansapura, J., Shanmukhappa, S. K., Lorenz, J. N., Osinska, H., Backer, K., Huby, A. C., Shrestha, A., Niss, O., Fleck, R.,

Quinn, C. T., Taylor, M. D., Purevjav, E., *et al.* (2016) Sickle cell anemia mice develop a unique cardiomyopathy with restrictive physiology. *Proc. Natl. Acad. Sci. U.S.A.* **113,** E5182–E5191 CrossRef Medline

33. Xu, W., Barrientos, T., Mao, L., Rockman, H. A., Sauve, A. A., and Andrews, N. C. (2015) Lethal cardiomyopathy in mice lacking transferrin receptor in the heart. *Cell Rep.* **13,** 533–545 CrossRef Medline
34. Loeven, A. M., Receno, C. N., Cunningham, C. M., and DeRuisseau, L. R. (2018) Arterial blood sampling in male CD-1 and C57BL/6J mice with 1% isoflurane is similar to awake mice. *J. Appl. Physiol.* **125,** 1749–1759 CrossRef Medline
35. Wilding, L. A., Hampel, J. A., Khoury, B. M., Kang, S., Machado-Aranda, D., Raghavendran, K., and Nemzek, J. A. (2017) Benefits of 21% oxygen compared with 100% oxygen for delivery of isoflurane to mice (*Mus musculus*) and rats (*Rattus norvegicus*). *J. Am. Assoc. Lab. Anim. Sci.* **56,** 148–154 Medline
36. Adelsperger, A. R., Bigiarelli-Nogas, K. J., Toore, I., and Goergen, C. J. (2016) Use of a low-flow digital anesthesia system for mice and rats. *J. Vis. Exp.* CrossRef Medline
37. Zolov, S. N., Bridges, D., Zhang, Y., Lee, W. W., Riehle, E., Verma, R., Lenk, G. M., Converso-Baran, K., Weide, T., Albin, R. L., Saltiel, A. R., Meisler, M. H., Russell, M. W., and Weisman, L. S. (2012) *In vivo*, Pikfyve generates PI(3,5)P2, which serves as both a signaling lipid and the major precursor for PI5P. *Proc. Natl. Acad. Sci. U.S.A.* **109,** 17472–17477 CrossRef Medline